Pressure-induced insulator-metal transition in a bilayer manganite: Pressure control of orbital stability

Y. Moritomo
Center for Integrated Research in Science and Engineering, Nagoya University, Nagoya 464-8601, Japan

K. Hirota
Department of Physics, Tohoku University, Sendai 980-8578, Japan

H. Nakao, T. Kiyama, and Y. Murakami
Photon Factory, Institute of Materials Structure Science, High Energy Accelerator Research Organization, Tsukuba 305-0801, Japan

S. Okamoto, S. Ishihara, and S. Maekawa
Institute for Materials Research, Tohoku University, Sendai 980-8577, Japan

M. Kubota and H. Yoshizawa
Neutron-Scattering Laboratory, Institute for Solid State Physics, University of Tokyo, Tokai, Ibaraki 319-1106, Japan
(Received 11 February 2000)

Pressure effects on transport as well as structural properties have been investigated for a bilayer manganite, $La_{2-2x}Sr_{1+2x}Mn_2O_7$ ($x=0.48$), near the phase boundary between the ferromagnetic metallic and the *A*-type antiferromagnetic states. An insulator-metal (IM) transition is found to be induced by applying pressure of ~ 0.7 GPa. On the basis of the synchrotron radiation x-ray structural analysis under high pressures, we have ascribed the IM transition to the variation of the stability of the e_g orbitals.

In perovskite-type transition-metal oxides, structural modification through the hydrostatic pressure and chemical substitution of the isovalent ions (*chemical* pressure) has significant effects on the magnetic and transport properties.[1–6] These two pressure effects are mediated by the variation of the structural parameters, which is usually regarded as control of the one-electron bandwidth W of the narrow d band through variation of the M-O-M bond angle (M is a transition metal). This simple picture has successfully explained effects of the hydrostatic as well as chemical pressures in $R\mathrm{NiO_3}$ (Ref. 1) and $(R,A)\mathrm{MnO_3}$,[2,5,6] where R and A are rare-earth and alkaline-earth metals, respectively. Nevertheless, we should recall that the pressure alters not only the W value, but also other physical quantities through variation of the structural parameters. In particular, in doped manganites with bilayer structure, $La_{2-2x}Sr_{1+2x}Mn_2O_7$,[7] several researchers[8–13] have proposed that the orbital stability of the degenerated e_g states governs the magnetic and electronic properties. Then, effects of hydrostatic pressure in this system have different aspects from those in $R\mathrm{NiO_3}$ and $(R,A)\mathrm{MnO_3}$.

The bilayer manganite $La_{2-2x}Sr_{1+2x}Mn_2O_7$ exhibits a planar ferromagnetic structure in the range $0.32 \leqslant x \leqslant 0.38$ at low temperatures, and does a canting between the neighboring ferromagnetic MnO_2 sheets above $x \sim 0.39$.[13–18] The magnetic structure becomes antiferromagnetic (A type) for $x \geqslant 0.48$. In the A-type bilayer manganites, the ferromagnetic MnO_2 sheet alternates along the c axis.[14–16] Such a magnetic structure is well understood in terms of the $d_{x^2-y^2}$ orbital state,[19] which causes the ferromagnetic double exchange interaction[20] within the MnO_2 sheet and antiferromagnetic superexchange coupling between the adjacent sheets (within the bilayer). With this magnetic structure, the e_g carriers are confined into the respective MnO_2 sheet due to the double exchange mechanism, which causes an upturn of the resistivity at lower temperature.[15] Kubota *et al.*[16] have systematically investigated the distortion of the MnO_6 octahedra, and have found a close correlation between the Jahn-Teller (JT) type distortion and magnetic structure. On the other hand, Akimoto *et al.*[13] have quantitatively investigated the stability of the $d_{3z^2-r^2}$ (or $d_{x^2-y^2}$) orbital by means of Madelung potential calculation[8] based on the structural parameters of $(La_{1-z}Nd_z)_{1.2}(Sr_{1-y}Ca_y)_{1.8}Mn_2O_7$ at a fixed hole concentration ($x=0.4$). They have found a strong interrelation between the orbital stability and the magnetic structure: with increase of the stability of the $d_{3z^2-r^2}$ orbital, the magnetic structure changes from A-type antiferromagnetic to ferromagnetic ones.

In this paper, we have investigated pressure effects on the transport as well as structural properties for a bilayer manganite, $La_{2-2x}Sr_{1+2x}Mn_2O_7$ ($x=0.48$), which shows the A-type spin ordering below $T_N=200$ K. Application of pressures is found to induce an insulator-metal (IM) transition. To comprehend the pressure-induced IM transition, we further have estimated the orbital stability through difference in the Madelung potential ΔV between the $d_{3z^2-r^2}$ and $d_{x^2-y^2}$ orbitals. We have found a close correlation between the resistivity behaviors and the ΔV values. Our high-pressure data indicate that the transport properties of bilayer manganites are governed by the orbital stability even under hydrostatic pressures.

Single crystals of $La_{2-2x}Sr_{1+2x}Mn_2O_7$ ($x=0.48$) were grown by the floating-zone method at a feeding speed of 10–20 mm/h. Stoichiometric mixture of commercial La_2O_3,

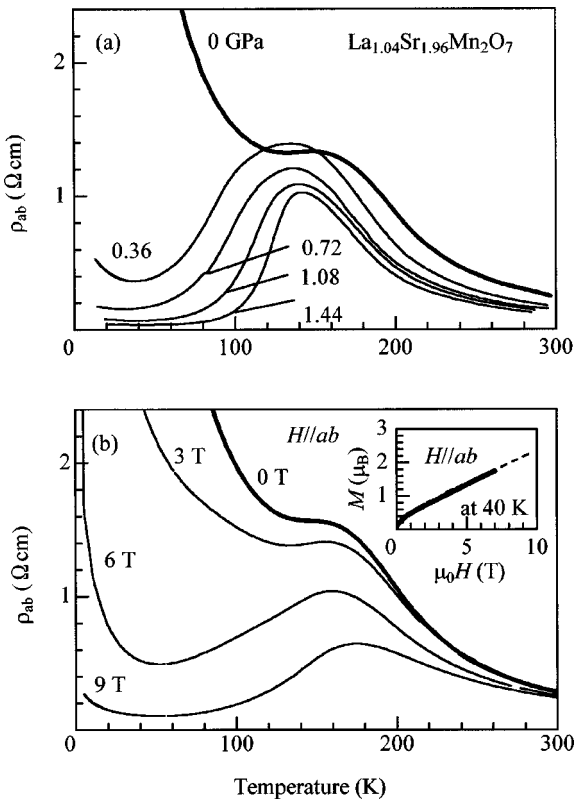

FIG. 1. (a) Hydrostatic pressure and (b) magnetic field effects on the in-plane component of resistivity ρ_{ab} of $La_{1.04}Sr_{1.96}Mn_2O_7$ ($x=0.48$). The pressure values are those measured at room temperature. Magnetic field was applied parallel to the ab plane. Inset shows the field dependence of the in-plane component M_{ab} of magnetization at 40 K ($H//ab$).

$SrCO_3$ and Mn_3O_4 powder was ground and calcined twice at 1250–1350 °C for 24 h. The resulting powder was pressed into a rod with a size of 5 mm$\phi\times$80 mm and sintered at 1350 °C for 48 h. The ingredient can be melted congruently in a flow of O_2. Single crystals, typically 4 mm in diameter and 10 mm in length, were obtained with two well-defined facets, which correspond to the crystallographic ab plane. The crystal symmetry is tetragonal ($I4/mmm$; $Z=2$) at ambient pressure without detectable impurities. A hydrostatic pressure was obtained with a clamp-type piston cylinder cell.[6] The in-plane component of resistivity (ρ_{ab}) was measured by the four-probe method using heat-treatment-type silver paint as electrodes. A small piece of crystal ($\sim 0.5\times 1\times 2\text{mm}^3$) was placed in a sample room, which was filled with silicone oil as a pressure-transmitting medium. The sample temperature was monitored with an AuFe(0.07%)-Chromel thermocouples attached at the pressure cell near the sample room. The pressure values quoted in this paper are those measured at room temperature. [The applied pressure relaxes at a rate of $-7\%/100$ K] Pressure-induced changes in the $\rho_{ab}-T$ curves were reproducible in repeated pressure cycles.

We show in Fig. 1(a) the in-plane component ρ_{ab} of resistivity of $La_{1.04}Sr_{1.96}Mn_2O_7$ ($x=0.48$) under various pressures. At ambient pressure ($P=0.0$ GPa; thick curve), the insulating behavior of ρ_{ab} is fairly suppressed at around T_N ($=200$ K), reflecting the long-range ferromagnetic spin ordering in the respective MnO_2 sheets (A-type structure). With further decrease of temperature, however, the $\rho_{ab}-T$ curve shows an upturn below ~ 120 K, due to the two-dimensional confinement of the e_g carriers. These resistivity behaviors are prototypical for a A-type bilayer manganite, and similar upturns of resistivity are observed in the other A-type bilayer manganites, $(La_{1-z}Nd_z)Sr_2Mn_2O_7$ ($x=0.5$).[15] Application of pressures significantly affects the resistivity behaviors, especially in the low-temperature region. At 1.44 GPa (1.08 GPa), the $\rho_{ab}-T$ curve shows a sharp drop below ~ 130 K (~ 120 K) and then monotonously decreases. The $\rho_{ab}-T$ curve at $P\geqslant 0.7$ GPa is reminiscent of that of ferromagnetic metallic (FM) $La_{0.12}Sr_{1.8}Mn_2O_7$ ($x=0.4$).[7] For comparision, we show in Fig. 1(b) magnetic field effects on ρ_{ab} of $La_{1.04}Sr_{1.96}Mn_2O_7$. Magnetic field was applied parallel to the ab plane. Under a field of 9 T, in which the low-temperature phase is nearly ferromagnetic [the in-plane component M_{ab} of magnetization is $\sim 2.2\mu_B$ at 40 K; see inset of Fig. 1(b)], the $\rho_{ab}-T$ curve shows a metallic behavior below ~ 160 K.[21] These suggest that the low-temperature phase at $P\geqslant P_c\sim 0.7$ GPa is FM.

To determine the variation of structural parameters under pressures, we have performed high-pressure x-ray experiments using a specially designed diamond-anvil cell (DAC) at room temperature. Synchrotron radiation (SR) x-ray source at Photon factory BL-1B was used with a cylindrical imaging plate as a detector, to obtain powder data of good counting statistics. Melt-grown crystal ingots were crushed into fine powder and were sealed in a gasket hole of the DAC, 0.1 mm in thickness and 0.3 mm in diameter, which was filled with ethanol/methanol mixture as a pressure-transmitting medium. Magnitude of the applied pressure were monitored by the position of the luminescence line R_1 (Ref. 22) from a small piece of ruby placed in the gasket hole. Precipitation method[23] was adopted in order to get a fine powder, which gives a homogeneous intensity distribution in the Debye-Scherrer powder ring. The wavelength of the incident x ray is 0.68975 Å, and the exposure time was for 30 min. We have analyzed thus obtained x-ray patterns with RIETAN-97β program,[24] and listed the prototypical results in Table I. The final refinements are satisfactory, in which R_{wp} is fairly typical of the published one ($R_{wp}=2-3\%$).

Figure 2(a) shows pressure dependence of the lattice constants, i.e., a and c, of $La_{1.04}Sr_{1.96}Mn_2O_7$. Error bars (0.1%) is due to misalignment of the DAC at respective pressures. Both the values decreases at a similar rate: $d\ln(a)/dP=-0.25\%/\text{GPa}$ and $d\ln(c)/dP=-0.20\%/\text{GPa}$. The lower panel of Fig. 2 shows pressure variation of the Mn-O bond lengths, $d_{\text{Mn-O1}}$, $d_{\text{Mn-O2}}$, and $d_{\text{Mn-O3}}$, calculated from the structural parameters. $d_{\text{Mn-O1}}$ and $d_{\text{Mn-O2}}$ are the out-of-plane bond lengths, while $d_{\text{Mn-O3}}$ is the in-plane one [see the inset of Fig. 2(b)]. At ambient pressure, the three Mn-O bond lengths are nearly the same ($\sim 1.97-1.99$ Å), causing the A-type magnetic ordering at low temperature via stabilization of the $d_{x^2-y^2}$ orbital. Surprisingly, application of pressure elongates the $d_{\text{Mn-O2}}$ value (apical oxygen): $d_{\text{Mn-O2}}\sim 2.0$ Å at ambient pressure, but becomes to ~ 2.1 Å above ~ 1.6 GPa. This makes a sharp contrast with the other two

TABLE I. Room-temperature structural parameters of $La_{2-2x}Sr_{1+2x}Mn_2O_7$ ($x=0.48$) at various pressures. The crystal symmetry is tetragonal ($I4/mmm$; $Z=2$). The atomic sites are: $A1$ $2b$ [0, 0, $\frac{1}{2}$], $A2$ $4e$ [0, 0, z], O1 $2a$ [0, 0, 0], O2 $4e$ [0, 0, z], O3 $8g$ [0, $\frac{1}{2}$, z], and Mn $4e$ [0, 0, z] (A: the site of rare-earth and alkaline-earth ions).

Pressure (GPa)	a (Å)	c (Å)	$A2(z)$	O2(z)	O3(z)	Mn(z)	R_{wp} (%)
1.3	3.8612(1)	19.9978(8)	0.31694(9)	0.1985(7)	0.0948(6)	0.0952(3)	2.51
2.2	3.8528(1)	19.9403(7)	0.31627(8)	0.1989(6)	0.0933(5)	0.0956(3)	2.42
3.6	3.8465(1)	19.9224(8)	0.31688(9)	0.2011(7)	0.0935(6)	0.0957(3)	2.96
4.2	3.83613(8)	19.8822(6)	0.31657(7)	0.2014(6)	0.0933(5)	0.0957(2)	2.72

bond lengths, i.e., $d_{\text{Mn-O1}}$ and $d_{\text{Mn-O3}}$, both of which show a negligible decrease with pressure. Such a pressure-induced distortion of the MnO_6 octahedra, that is, five short and one long Mn-O bonds, does not change the W value, but significantly stabilizes the $d_{3z^2-r^2}$ orbital. Incidentally, Arygriou *et al.*[25] have investigated pressure-induced variation of the Mn-O bondlengths of FM $La_{1.2}Sr_{1.8}Mn_2O_7$ ($x=0.4$) with use of a pulsed neutron source. Similarly to the present case, they have observed elongation of $d_{\text{Mn-O2}}(\sim 1\%/\text{GPa})$ as well as contraction of $d_{\text{Mn-O1}}$ and $d_{\text{Mn-O3}}$ at 300 K.

The orbital stability can be evaluated by the Madelung potentials calculations.[8,9,13] The Madelung potentials acting on a hole in the $d_{x^2-y^2}$ and $d_{3z^2-r^2}$ orbitals are given by

$$V(d_{x^2-y^2})=V(\vec{r}_0+r_d\hat{x})$$

and

$$V(d_{3z^2-r^2})=[V(\vec{r}_0+r_d\hat{z})+V(\vec{r}_0-r_d\hat{z})]/2,$$

respectively. Here $\vec{r}_0$ indicates the position of the Mn ion and r_d (=0.42 Å) is the radius where the radial charge density of the $3d$ orbital becomes maximum. $\hat{x}$ and $\hat{z}$ are the unit vectors along the crystallographic a and c axes, respectively. Based on the structural parameters, we have calculated pressure variation of difference in the Madelung potentials $\Delta V[=V(d_{3z^2-r^2})-V(d_{x^2-y^2})]$ between two e_g orbitals. The results are plotted in Fig. 3 against applied pressures. With increase of pressure, the ΔV value (closed circles) gradually increases, and hence the $d_{3z^2-r^2}$ orbital becomes stable. Such a pressure variation of the ΔV value qualitatively explains the pressure-induced IM transition, because the stabilized $d_{3z^2-r^2}$ orbital favors the FM state.

Finally, let us compare the present pressure effects on the orbital stability with the *chemical* pressure effects.[13] In the inset of Fig. 3, we show experimentally obtained magnetic phase diagram of $(La_{1-z}Nd_z)_{1.2}(Sr_{1-y}Ca_y)_{1.8}Mn_2O_7$ against

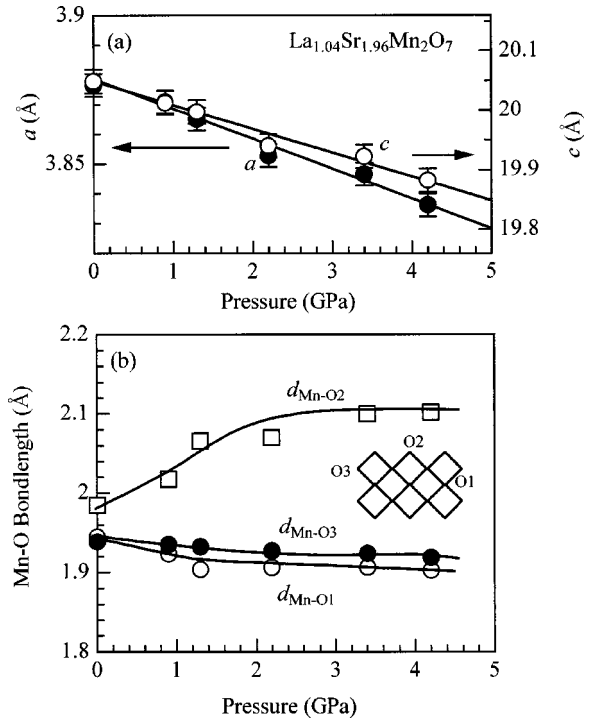

FIG. 2. Pressure dependence of (a) lattice constants, a and c, and (b) the Mn-O bondlengths, $d_{\text{Mn-O1}}$, $d_{\text{Mn-O2}}$, and $d_{\text{Mn-O3}}$, of $La_{1.04}Sr_{1.96}Mn_2O_7$ ($x=0.48$) at 300 K. Error bars (0.1%) are due to misalignment of the DAC at respective pressures. Positions of the independent oxygen sites, i.e., O1, O2, and O3, are schematically shown in (b).

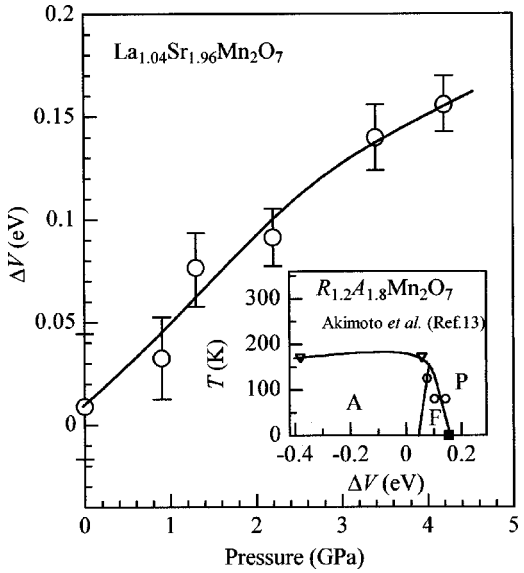

FIG. 3. Pressure variation of difference in the Madelung potentials ΔV $[\equiv V(d_{3z^2-r^2})-V(d_{x^2-y^2})]$, where $V(d_{3z^2-r^2})$ $[V(d_{x^2-y^2})]$ is the Madelung potential for the $d_{3z^2-r^2}$ ($d_{x^2-y^2}$) hole. The $d_{3z^2-r^2}$ orbital becomes stable as ΔV increases. Inset (cited from Ref. 13) shows magnetic transition temperatures of $(La_{1-z}Nd_z)_{1.2}(Sr_{1-y}Ca_y)_{1.8}Mn_2O_7$ against ΔV. Circles and triangles stand for Curie temperature T_C, Néel temperature T_N, respectively. F, A, and P represent ferromagnetic metallic, A-type antiferromagnetic, and paramagnetic states, respectively.

ΔV (cited from Ref. 13). Circles and triangles stand for Curie temperature T_C and Néel temperature T_N, respectively. F, A, and P means ferromagnetic, *A*-type antiferromagnetic, and paramagnetic states, respectively. If one sees the phase diagram from left to right (the $d_{3z^2-r^2}$ orbital is stabilized), the magnetic structure changes from A to F, and finally the P state appears. In the point of the orbital stability, the present compound ($\Delta V \sim 0.01$ at ambient pressure) locates in the *A* phase near the F-A phase boundary. Application of pressure significantly enhances the ΔV value at a rate of ~ 0.05 eV/GPa. Then, the pressurized compound could go beyond the A-F phase boundary at ~ 1 GPa, which is consistent with the experimentally obtained value [$P_c \sim 0.7$ GPa; see Fig. 1(a)].

In summary, we have investigated pressure effects on the structural parameters of $La_{2-2x}Sr_{1+2x}Mn_2O_7$ ($x=0.48$), which shows the IM transition at $P_c \sim 0.7$ GPa. The Madelung potential calculation (ΔV) based on the structural parameters has revealed that the orbital stability governs the magnetic and transport properties of bilayer manganites even under hydrostatic pressures. Thus high-pressure structural analysis is a powerful tool to reveal the complicated phenomena induced by pressures even in the strongly correlated electron systems.

The authors are grateful to E. Nishibori and K. Kato for their help in powder preparation for the SR x-ray measurements. This work was supported by a Grant-In-Aid for Scientific Research from the Ministry of Education, Science, Sports and Culture.

[1] J. B. Torrance, A. Marbeuf, M. Pouchard, and P. Hagenmuller, Phys. Rev. B **45**, 8209 (1992).
[2] H. Y. Hwang, S.-W. Cheong, P. G. Radaeli, M. Marezio, and B. Batlogg, Phys. Rev. Lett. **75**, 914 (1995); H. Y. Hwang, T. T. M. Palstra, S.-W. Cheong, and B. Batlogg, Phys. Rev. B **52**, 15 046 (1995).
[3] X. Obradors, L. M. Paulius, M. B. Maple, J. B. Torrance, A. I. Nazzal, I. Fontcuberta, and X. Granados, Phys. Rev. B **47**, 12 353 (1993).
[4] P. L. Canfield, J. D. Thompson, S.-W. Cheong, and L. W. Rupp, Phys. Rev. B **47**, 12 357 (1993).
[5] Y. Moritomo, A. Asamitsu, and Y. Tokura, Phys. Rev. B **51**, 16 491 (1995); **56**, 12 190 (1997).
[6] Y. Moritomo, H. Kuwahara, Y. Tomioka, and Y. Tokura, Phys. Rev. B **55**, 7549 (1997).
[7] Y. Moritomo, A. Asamitu, H. Kuwahara, and Y. Tokura, Nature (London) **380**, 141 (1996).
[8] S. Ishihara, S. Okamoto, and S. Maekawa, J. Phys. Soc. Jpn. **66**, 2965 (1997).
[9] S. Okamoto, S. Ishihara, and S. Maekawa, cond-mat/9909321 (unpublished).
[10] R. Maezono and N. Nagaosa, Phys. Rev. B **61**, 1825 (2000).
[11] J. van den Brink and D. Khomskii, Phys. Rev. Lett. **82**, 1016 (1999).
[12] Y. Moritomo, Y. Maruyama, T. Akimoto, and A. Nakamura, J. Phys. Soc. Jpn. **67**, 405 (1997).
[13] T. Akimoto, Y. Moritomo, K. Ohoyama, S. Okamoto, S. Ishihara, S. Maekawa, and A. Nakamura, Phys. Rev. B **59**, R14 153 (1999); T. Akimoto, Y. Moritomo, K. Ohoyama, S. Okamoto, S. Ishihara, S. Maekawa, K. Hirota, and A. Nakamura, Phys. Rev. B (to be published).
[14] K. Hirota, Y. Moritomo, H. Fujioka, M. Kubota, H. Yosizawa, and Y. Endoh, J. Phys. Soc. Jpn. **67**, 3380 (1998).
[15] Y. Moritomo, A. Nakamura, K. Ohoyama, M. Ohasi, and K. Hirota, J. Phys. Soc. Jpn. **68**, 631 (1999).
[16] M. Kubota, H. Yoshizawa, K. Hirota, H. Fujioka, Y. Endoh, and Y. Moritomo, J. Phys. Chem. Solids **60**, 1161 (1999); M. Kubota, H. Fujioka, K. Hirota, K. Ohoyama, Y. Moritomo, H. Yoshizawa, and Y. Endoh, cond-mat/9902288, J. Phys. Soc. Jpn. (to be published).
[17] J. F. Mitchell, D. N. Argyriou, J. D. Jorgensen, D. G. Hinks, C. D. Potter, and S. D. Bader, Phys. Rev. B **55**, 63 (1997).
[18] D. N. Argyriou, J. F. Mitchell, C. D. Potter, S. D. Bader, R. Kleb, and J. D. Jorgensen, Phys. Rev. B **55**, R11 965 (1997); D. N. Argyrou, J. F. Mitchell, P. G. Radaell, H. N. Bordallo, D. E. Cox, M. Medarde, and J. D. Jorgensen, *ibid.* **59**, 8695 (1999).
[19] T. Akimoto, Y. Maruyama, Y. Moritomo, A. Nakamura, K. Hirota, K. Ohoyama, and M. Ohashi, Phys. Rev. B **57**, R5594 (1998); Y. Moritomo, T. Akimoto, A. Nakamura, K. Ohoyama, and M. Ohashi, *ibid.* **58**, 5544 (1998).
[20] P. W. Anderson and H. Hasagawa, Phys. Rev. **100**, 675 (1955).
[21] Upturn at ~ 40 K is perhaps due to residual *A*-type component.
[22] H. K. Mao and P. M. Bell, Science **200**, 1145 (1978).
[23] M. Takata, E. Nishibori, K. Kato, M. Sakata, and Y. Moritomo, J. Phys. Soc. Jpn. **68**, 2190 (1999).
[24] F. Izumi, *The Rietveld Method*, edited by R. A. Young (Oxford University Press, Oxford, 1993), Chap. 13; Y.-I. Kim and F. Izumi, J. Ceram. Soc. Jpn. **102**, 401 (1994).
[25] D. N. Argyriou, J. F. Mitchell, J. B. Goodenough, O. Chmaissem, S. Short, and J. D. Jorgensen, Phys. Rev. Lett. **78**, 1568 (1997).